Proc. Natl. Acad. Sci. USA
Vol. 90, pp. 9770–9777, November 1993
Colloquium Paper

This paper was presented at a colloquium entitled "Images of Science: Science of Images," organized by Albert V. Crewe, held January 13 and 14, 1992, at the National Academy of Sciences, Washington, DC.

Color, contrast sensitivity, and the cone mosaic

DAVID WILLIAMS*, NOBUTOSHI SEKIGUCHI†, AND DAVID BRAINARD‡

Center for Visual Science, University of Rochester, Rochester, NY 14627-0270

ABSTRACT **This paper evaluates the role of various stages in the human visual system in the detection of spatial patterns. Contrast sensitivity measurements were made for interference fringe stimuli in three directions in color space with a psychophysical technique that avoided blurring by the eye's optics including chromatic aberration. These measurements were compared with the performance of an ideal observer that incorporated optical factors, such as photon catch in the cone mosaic, that influence the detection of interference fringes. The comparison of human and ideal observer performance showed that neural factors influence the shape as well as the height of the foveal contrast sensitivity function for all color directions, including those that involve luminance modulation. Furthermore, when optical factors are taken into account, the neural visual system has the same contrast sensitivity for isoluminant stimuli seen by the middle-wavelength-sensitive (M) and long-wavelength-sensitive (L) cones and isoluminant stimuli seen by the short-wavelength-sensitive (S) cones. Though the cone submosaics that feed these chromatic mechanisms have very different spatial properties, the later neural stages apparently have similar spatial properties. Finally, we review the evidence that cone sampling can produce aliasing distortion for gratings with spatial frequencies exceeding the resolution limit. Aliasing can be observed with gratings modulated in any of the three directions in color space we used. We discuss mechanisms that prevent aliasing in most ordinary viewing conditions.**

There has been considerable recent interest in understanding how color and luminance information are processed in the visual system. It is well known that the mechanisms sensitive to chromatic modulation have inferior resolution to those sensitive to luminance modulation (1), but the reasons why this is so are not yet clear. This paper examines the role of the first few stages of the visual system in detecting spatial patterns that vary in chromaticity or luminance. Wilson Geisler (2) has developed an elegant computational approach to this problem based on the theory of ideal observers. We describe an ideal observer similar to Geisler's and use it to examine the effect on contrast sensitivity of optical factors such as those associated with the cone mosaic. We then compare ideal observer performance with new measurements of human contrast sensitivity for patterns modulated in different color directions. This comparison reveals the properties of the neural mechanisms that underlie human performance. This paper summarizes work described by Sekiguchi *et al.* (3, 4) to which readers are referred for details of the psychophysical experiments and computational model.

The publication costs of this article were defrayed in part by page charge payment. This article must therefore be hereby marked "*advertisement*" in accordance with 18 U.S.C. §1734 solely to indicate this fact.

Stimuli for Measuring Ideal and Human Contrast Sensitivity

We computed the contrast sensitivity of the ideal observer and measured the contrast sensitivity of human observers with the same stimulus set. For the ideal observer, analytic descriptions of the stimuli were used as input to a computational model; for the human observers, the stimuli were generated with a dual laser interferometer (3).

We measured performance with sinusoidal gratings that were modulated in one of three directions in color space. The particular directions we used corresponded closely to directions considered to be cardinal in color space (5). We used a red–green isoluminant interference fringe, an isochromatic yellow interference fringe, and a violet fringe seen only by the short-wavelength-sensitive (S) cones. The stimuli are shown in Fig. 1. The intensity profile at the top of the figure shows the configuration used to measure both isochromatic and red–green isoluminant contrast sensitivity. A red (632.8 nm) and a green (514.5 nm) interference fringe of the same spatial frequency, orientation, and luminance were added together and drifted in opposite directions at 0.25 Hz. When the fringes were out of phase, a red–green isoluminant stimulus was produced. When they were in phase, a yellow isochromatic stimulus was produced. Sekiguchi *et al.* (3) showed that observers can set contrast thresholds that provide valid estimates of both red–green isoluminant and isochromatic contrast sensitivity while viewing this single time-varying stimulus. The advantage of drifting the red and green gratings is that it avoids the need to keep them in register. This phase locking becomes progressively more difficult at higher spatial frequencies due to head movements and transverse chromatic aberration. The fringes are superimposed on a yellow background sufficiently bright that the masking effect of laser speckle was negligible (3, 6).

Fig. 1*a* shows the profile of a violet grating superimposed on a yellow background, which modulates the S cones but produces a negligible luminance modulation. The contrast of the violet grating was temporally modulated at 0.5 Hz so that its temporal properties matched those of the stimuli in the other color directions. For all color directions, the intensity profile of each fringe was multiplied by a Gaussian window to restrict the stimulus to a constant number of cycles at all spatial frequencies. Over the range of spatial frequencies we used, the grating summation area for all color directions was about 5 cycles within ±2 standard deviations of the Gaussian

Abbreviations: S, M, and L cones, short-, medium-, and long-wavelength-sensitive cones, respectively; CSF, contrast sensitivity function; MTF, modulation transfer function; c/deg, cycle per degree.

*To whom reprint requests should be addressed at: Center for Visual Science, University of Rochester, 274 Meliora Hall, Rochester, NY 14627-0270.
†Present address: Olympus Optical Co., Ltd., 2-3 Kuboyama, Hachioji, Tokyo, Japan.
‡Present address: Department of Psychology, University of California, Santa Barbara, CA 93106.

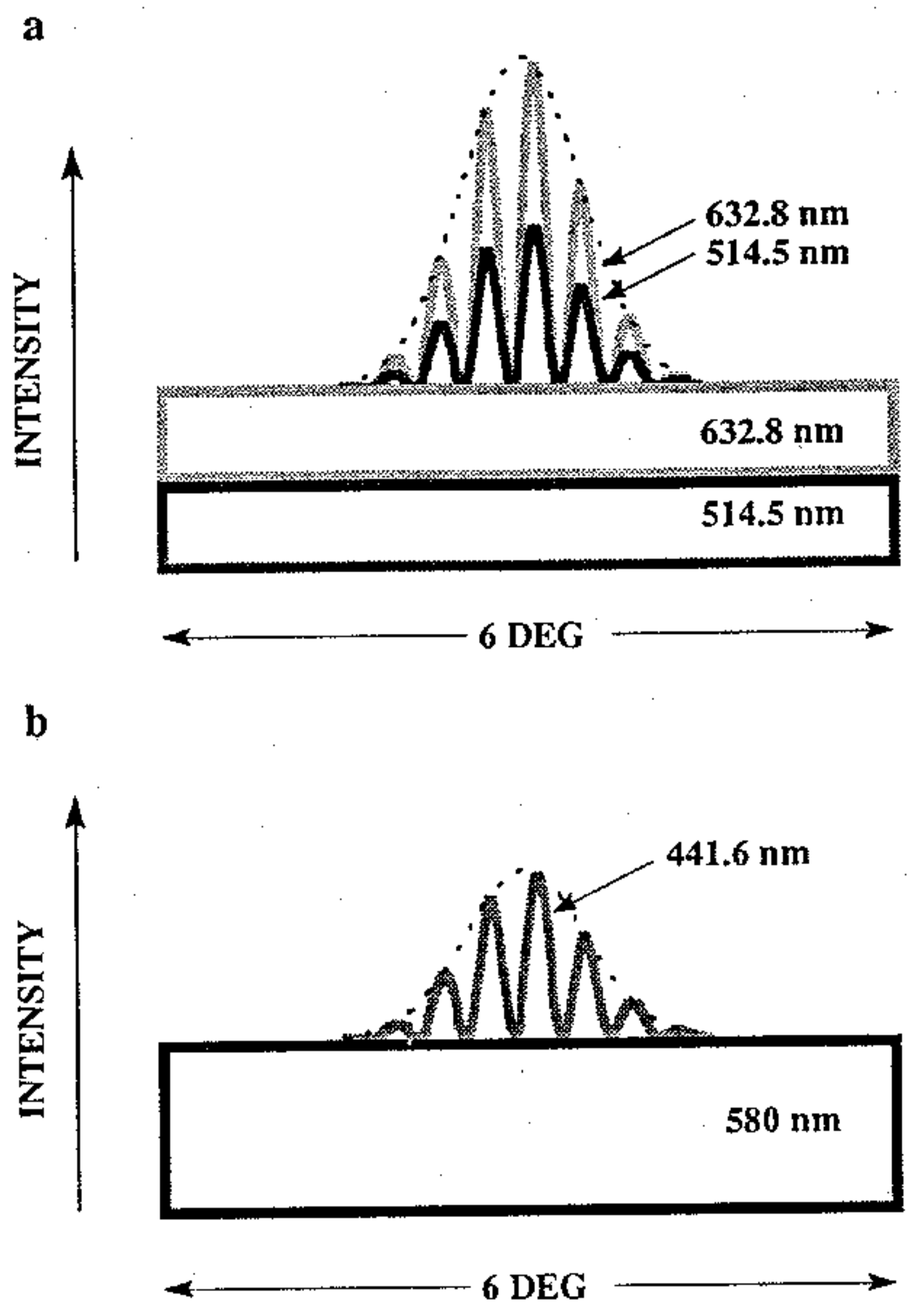

FIG. 1. (*a*) Intensity profile shows the configuration that produced the isochromatic and red–green isoluminant interference fringes. The retinal illuminance was 500 trolands (td; 1 td = 1 lumen per m^2 for an area of the entrance pupil of 1 mm^2. (*b*) The profile shows the violet interference fringe superimposed on a yellow background, which was seen only with S cones. The violet fringe had a retinal illuminance of 2.6 td. Additional experimental details can be found in Sekiguchi *et al.* (3, 4). DEG, degrees.

(4). We used gratings of this size for all conditions. This ensured that the grating summation area did not influence the comparison of human performance for different color directions. It also tended to make human performance agree more closely with ideal performance, since the ideal observer integrates spatial information perfectly at any field size while humans do not.

Ideal Observer Analysis of the Role of the Cone Mosaic

Components of the Ideal Observer. The ideal observer had the optical properties of the eye and of the cone mosaic that we have good reason to expect in a human observer viewing laser interference fringes. Fig. 2 *Right* shows the stages of the ideal observer we implemented. The details of this model can be found in Sekiguchi *et al.* (4), which was borrowed in great measure from that originally developed by Geisler (2). Unlike Geisler's ideal observer, there is no stage corresponding to blurring by the cornea, pupil, and lens because laser interferometry avoids these effects. This offers a simplification in the comparison of ideal and human performance, because uncertainties about the optical quality of the human eye are avoided.

Ocular media. The absorption of light by the ocular media, such as the lens and the macular pigment, was incorporated using estimates from Wyszecki and Stiles (7).

Cone blurring. The apertures of cones, which introduce minor blurring of the retinal image, were assumed to be Gaussian with a full width at half height that was 34% of the distance to each cone's nearest neighbors (8, 9).

Mosaic photon loss. The quantum efficiency of the retina depends on the size and spacing of the three cone classes. Two cone mosaics were used in the analysis, corresponding to the two retinal locations where contrast sensitivity measurements were made on human observers. In addition to the fovea, a location 1 degree in the parafovea was used because we wished to measure human performance where S-cone density is highest. The coordinates of individual cones were taken from histological sections of monkey retina (provided by Hugh Perry, University of Oxford) for the fovea and human retina (provided by Christine Curcio, University of Alabama) and for the parafoveal location. We assumed that 5% of the cones were S cones (10) and that the ratio of long-wavelength-sensitive (L) to middle-wavelength-sensitive (M) cones was 2 to 1. The three cone photopigments were randomly assigned in these proportions to the cone locations in each mosaic. We estimate that rods account for <4% of the light collecting area at either retinal location we used, so we ignored their effects.

Cone photopigments. The cone spectral sensitivities used were the action spectra obtained from suction electrode recordings of single primate cones (11), with maximum sensitivities at 430, 531, and 561 nm.

Ideal discriminator. The ideal observer model can be evaluated with any number of the optical stages included. This is illustrated with the dotted lines that run to the circles labeled ID for ideal discriminator. The ideal discriminator is a maximum-likelihood decision rule (2) that, for each stimulus, has exact knowledge of the probability distribution of photons across all the cones. The stimuli used in the analysis had no phase uncertainty but were subject to photon noise. The ideal observer's task was a two-interval forced choice. The threshold contrast of the stimulus was calculated with a sensitivity index (d') of 0.96. The temporal integration time for the ideal observer was 1 sec.

Performance of the Ideal Observer. The contrast sensitivity functions (CSFs) in Fig. 2 *Left* illustrate the effect of each of the stages of the ideal observer. Geisler (2) provides an excellent review of these effects. If the ideal discriminator is placed after the first stage in the model, the resulting CSF has a slope of −1. This is so because the size of the fringe patch is inversely proportional to spatial frequency, so that fewer photons are available to indicate the presence of the stimulus at high than at low spatial frequencies. The absorption of light by the ocular media reduces the number of photons available for the detection task uniformly at all spatial frequencies, causing a downward vertical shift in the CSF without a change in shape.

The cone mosaic has two effects. (*i*) Because each cone integrates photons over a finite area, some information is lost about the locations of photons in the retinal image (6, 8, 12, 13). This produces a small additional loss in contrast sensitivity at high spatial frequencies. (*ii*) The efficiency of the ideal observer depends on the total photon catch of the mosaic, which is proportional to the product of the area of the cone aperture and the density of receptors. The loss of photons between the receptors reduces the ideal observer's efficiency equally at all spatial frequencies, producing a uniform downward shift in the CSF.

If one maintains a fixed density of receptors with fixed apertures, then the packing arrangement of these photoreceptors in the mosaic typically has very little effect on the performance of the ideal observer. We explored several packing geometries ranging from a random assignment rule to a regular packing geometry. All produced essentially the same ideal observer performance. (This need not always be true: for example, if the receptors all happened to lie at the nodes of an interference fringe, the ideal observer would be incapable of detecting it at any contrast. However, this kind of situation tends not to arise in the human visual system where the cone mosaic always has some disorder.)

The last stage of the ideal observer, the cone photopigments, has an effect similar to that of the ocular media and the

photon catch of the mosaic. For a stimulus with a given wavelength composition, the photopigments influence only the vertical position of the CSF, depending on how efficiently they absorb photons. Note that all the stages in the ideal observer prior to the decision stage are optical. The ideal observer we constructed does not include any subsequent neural stages. These neural factors are indicated in Fig. 2, where they cause the human observer's contrast sensitivity to interference fringes to lie well below the ideal CSF.

Fig. 3 shows the performance of the ideal observer in the fovea and in the parafovea for stimuli in the three color directions. An important observation (2) is that though the color direction affects the vertical position of the CSF, it does not affect its shape. The cone aperture is the only factor that causes the shape of the CSF to depart from a line of −1 slope, and its effect does not depend on stimulus color direction. Indeed, the cone aperture produces almost no effect over the range of spatial frequencies plotted in Fig. 3. That neither the packing geometry nor the density of receptors (assuming a fixed aperture) affects the shape is consistent with earlier conclusions about the role of the cone mosaic in human vision (2, 6, 14, 15). We will see later that for the human observer (but not the ideal observer) sampling by the cone mosaic together with neural factors can influence contrast sensitivity at spatial frequencies above the resolution limit. But any differences in the shape of contrast sensitivity functions measured on human observers at lower spatial frequencies must be due to neural factors.

The effect of the density of receptors on the vertical position of ideal observer CSF is illustrated by the large reduction in parafoveal S-cone contrast sensitivity relative to the parafoveal isochromatic CSF. Due to their low density, the S cones catch fewer photons than the numerous M and L cones, which mediate isochromatic contrast sensitivity, reducing S-cone contrast sensitivity uniformly at all spatial frequencies.

The red–green isoluminant CSF is uniformly shifted below the isochromatic CSF (2). This shift is not related to the numbers of cones, since the same numbers of M and L cones are involved in both tasks. Nor is it caused by the wavelength composition of the two types of stimuli, which is identical for the two tasks. Rather, detection of red–green isoluminant fringes is hindered by the extensive overlap in the spectral sensitivities of the two cone classes. Consider the contrast seen by either of the two cone classes exposed to a red–green isoluminant stimulus of maximum contrast. The overlap in spectral sensitivities implies that each cone class will respond to both the red and green components of the stimulus, reducing the modulation of each cone class below that produced by an isochromatic stimulus.

The Role of Neural Factors in Contrast Sensitivity

To evaluate the neural mechanisms that influence human visual performance, one must remove optical effects from contrast sensitivity measurements. With the use of laser interferometry, we have removed some of these optical effects experimentally, namely, those associated with blurring by the eye's optics. Unfortunately, there is no technique comparable to interferometry that would allow us to bypass the cone mosaic. However, the optical effects of the cone mosaic obtained with the ideal observer calculations can be backed out of human contrast sensitivity measurements to isolate the spatial properties of purely neural mechanisms. This analysis is appropriate to the extent that the ideal observer captures all the relevant optical effects of the ocular media, the cone mosaic, and cone photopigments.

Performance of Human Observers. Fig. 4 *Upper* shows foveal isochromatic and red–green isoluminant CSFs for three observers. The ordinate is based on the equivalent contrast metric of Jordan *et al.* (16). In this case, the use of this ordinate is tantamount to correcting for the effect of the overlap in the M- and L-cone spectral sensitivities. Fig. 4 *Lower* shows the ratio of human to ideal performance for the three observers. All the curves are concave downward, indicating that the neural efficiency of human observers declines both at low and at high spatial frequency for both red–green isoluminant and isochromatic color directions.

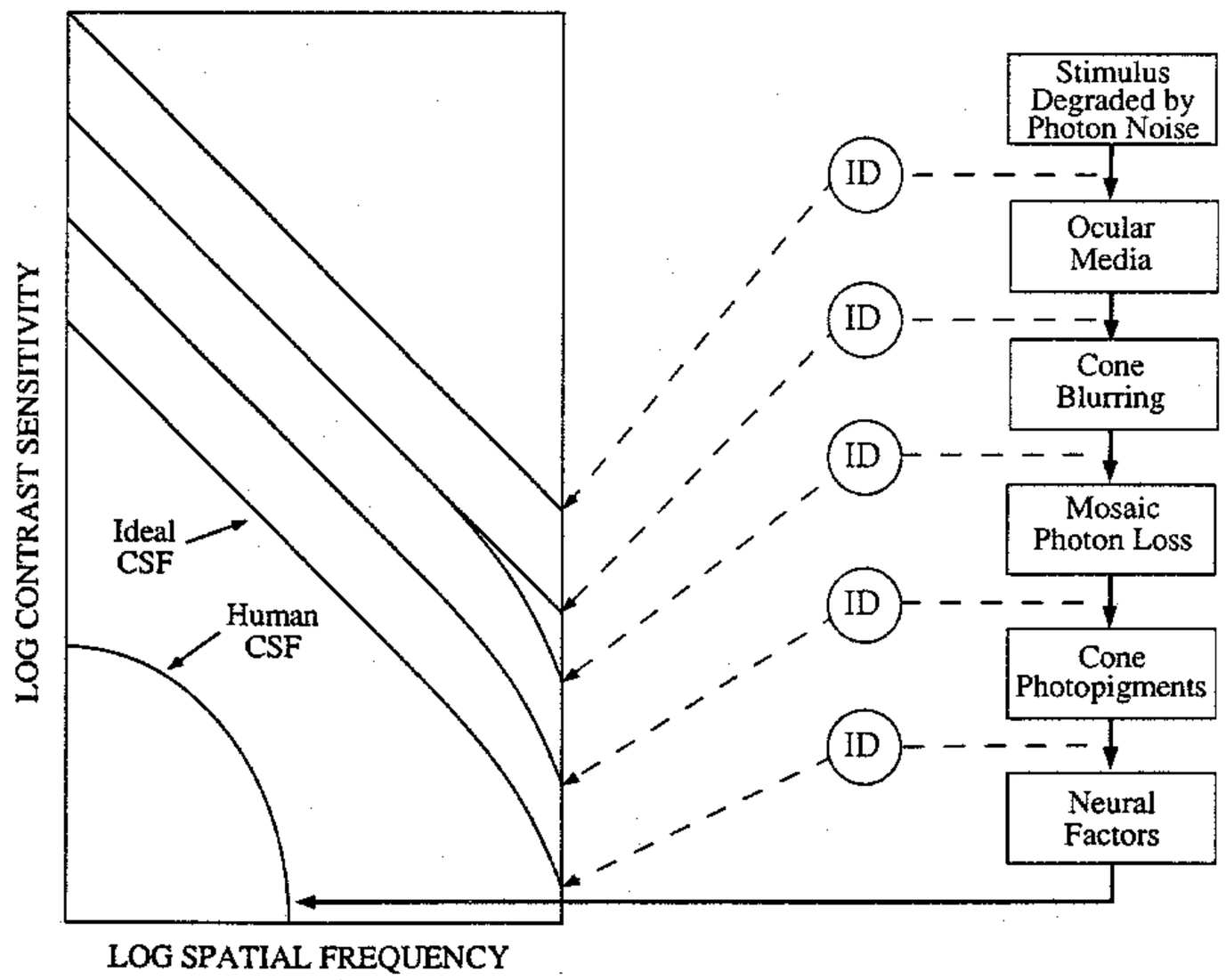

FIG. 2. (*Right*) Components of the ideal observer model. (*Left*) Qualitative influence of each component on ideal contrast sensitivity. The circles containing ID represent the final stage of the ideal observer, the ideal discriminator, that can be placed at various points to determine the effect of each stage. The ideal CSFs that were ultimately compared with human CSFs included all stages up to that labeled "neural factors." This last stage represents a number of factors that affect human contrast sensitivity alone.

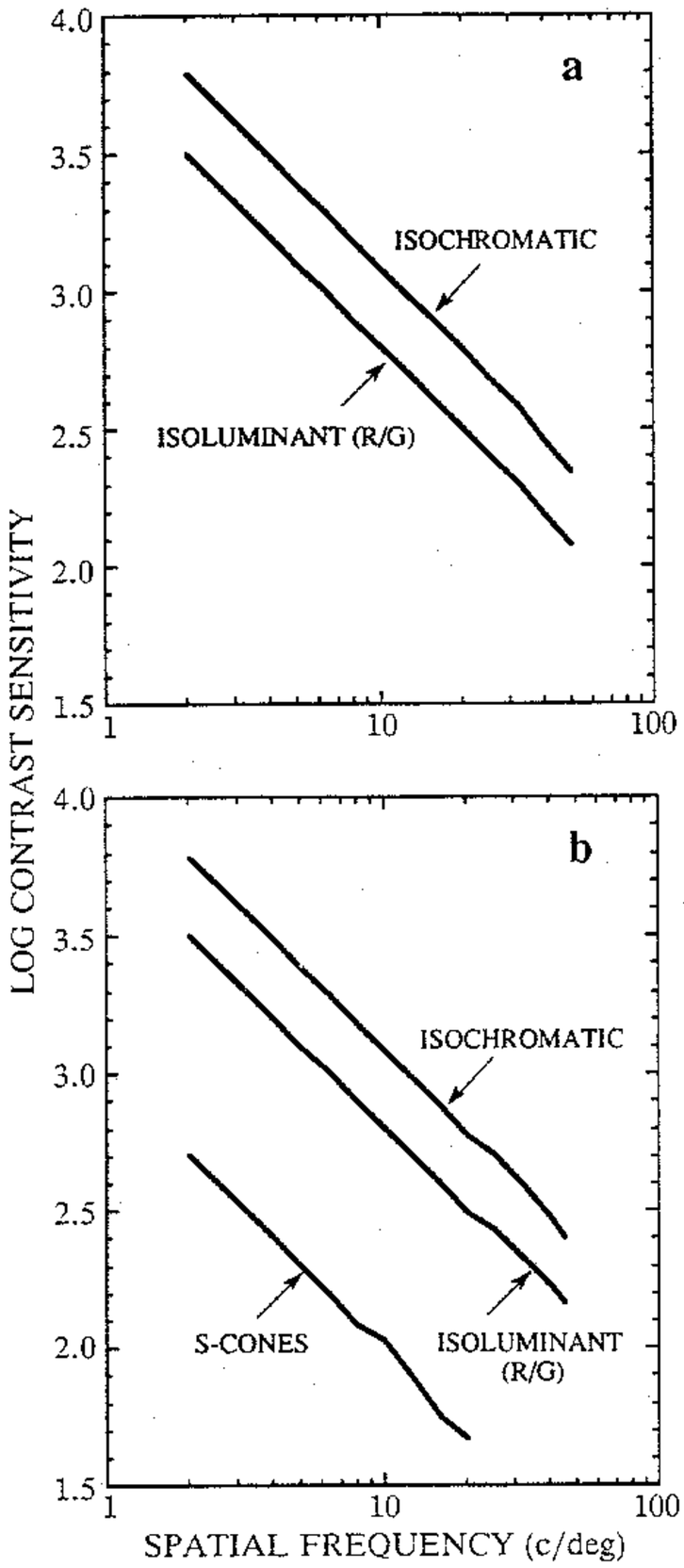

FIG. 3. Performance of the ideal observer for different color directions in the fovea (*a*) and parafovea (*b*). R/G, red/green; c/deg, cycles per degree.

At low frequencies, neural efficiency drops for red–green isoluminant contrast sensitivity, though it is less dramatic than for the isochromatic case. The dynamic range of luminance variations in the environment, produced by changes in ambient illumination, is probably considerably higher than the dynamic range of chromatic variation. To cope with this larger dynamic range, the visual system may have incorporated an additional adaptation mechanism for isochromatic stimuli to avoid saturation. Such a mechanism would be expected to produce an additional loss of efficiency particularly at low spatial frequencies because illumination changes predominantly affect these components of the spectra of natural scenes.

It is often suggested that chromatic mechanisms are strictly low-pass, but the drop in their neural efficiency functions at low spatial frequencies leaves room for some lateral inhibition in the red–green chromatic pathway, though it may be less strong than in the pathways serving isochromatic stimuli.

There is a clear decline at high spatial frequencies even for the isochromatic case, contrary to the conclusion of Banks *et al.* (17). They suggested that only optical factors were required to explain the shape of the foveal isochromatic CSF, while our conclusion is that at high spatial frequencies additional neural factors are implicated. The conclusions of Banks *et al.* (17) were based on contrast sensitivity measurements obtained with incoherent gratings, and they may have overestimated the amount of blurring of such stimuli by the eye's optics. They also may have somewhat overestimated the blurring by the cone aperture: they assumed that the cone aperture was as large as the spacing between cones. The present study used interference fringes, which are immune to optical blurring (8), and incorporated recent smaller psychophysical estimates of the size of the foveal cone aperture (8).

At high spatial frequencies, the fall-off in efficiency is more rapid for red–green isoluminant than for isochromatic stimuli, indicating a difference in the spatial bandwidth of the neural mechanisms that respond to these two color directions. Fig. 5 shows the same results as in Fig. 4 but the spatial frequencies corresponding to the red–green isoluminant data have been multiplied by a factor of 1.8, which amounts to sliding these data rightward by 0.25 log unit. This brings the two sets of data into register at mid-to-high spatial frequencies for all three observers, suggesting that the neural mechanism that detects red–green isoluminant signals has a bandwidth that is about half that of the mechanism that detects isochromatic signals.

Fig. 6 shows the parafoveal S-cone contrast sensitivity data compared with the parafoveal red–green isoluminant contrast sensitivity data for two observers. The S-cone data have been shifted upward relative to the red–green isoluminant data in accordance with the calculations of the ideal observer. As described above, the sparse density of the S cones in the mosaic impairs S-cone contrast sensitivity uniformly at all spatial frequencies simply by reducing quantum catch. Once this impairment is corrected for, there is a striking agreement between the two sets of data. This indicates that the spatial bandwidth is the same for chromatic mechanisms that detect these two color directions and that the neural components of these mechanisms are equally efficient. Why this should be true is not clear. In normal viewing, both chromatic aberration and the low density of S cones tend to reduce spatial performance for S-cone stimuli relative to that for M- and L-cone isoluminant stimuli. In the evolution of the visual system, one might expect neural mechanisms beyond the receptors to have evolved to match the limitations imposed by earlier stages. In that case, the spatial bandwidth for S-cone stimuli ought to be somewhat smaller than that for red–green isoluminant stimuli. The fact that it is not hints that some other organizational principle is at work. Whatever that principle is, these results emphasize the similarity in the neural mechanisms that respond to color changes, contrasting them with those that respond to luminance variations.

To better visualize these neural effects, it is helpful to assume that the observed neural losses are caused by a linear spatial filter, followed by additive neural noise. One can then estimate what Gaussian point spread functions would produce the observed losses in contrast sensitivity at high frequencies. (We ignore here the losses at low frequencies that occur, for example, in isochromatic contrast sensitivity.) Fig. 7 shows these estimates for the foveal contrast sensitivity measurements. The hypothetical point spread function underlying the detection of red–green isoluminant interference fringes has a full width at half height of 1.5 min, roughly twice the width of the isochromatic point spread function. The isochromatic point spread is >3 times the size of a single foveal cone aperture but is comparable in size to the point spread function of the optics of the eye (18). Apparently, optical and neural blurring are roughly the same in the fovea. This makes some sense from an evolutionary perspective, since there would be little selection pressure for one to be dramatically different from the other.

Aliasing and Visual Resolution

The ideal observer analysis described above evaluates the effect of optical stages on the detection of spatial patterns. Human observers not only detect spatial patterns but also

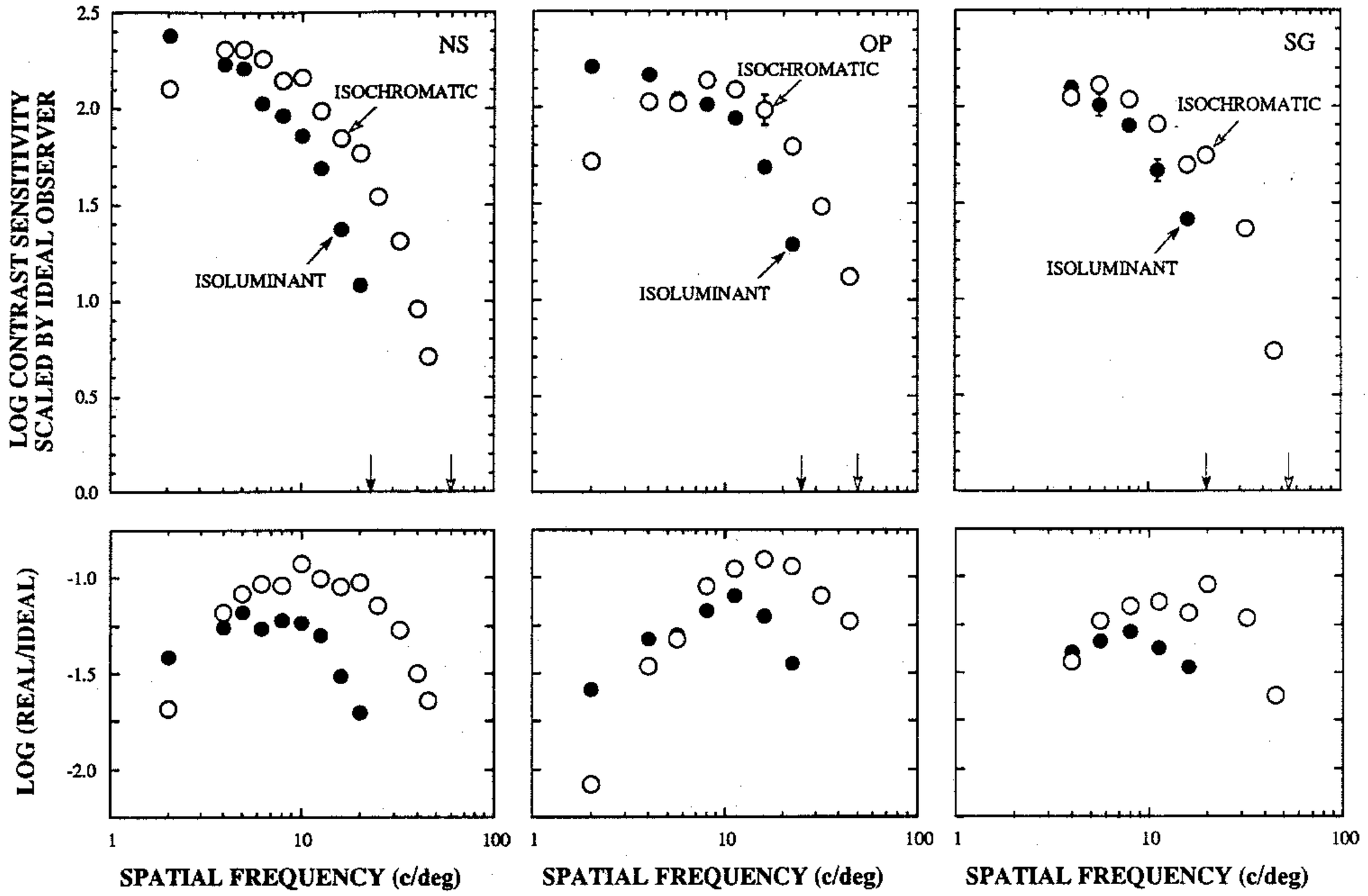

FIG. 4. (*Upper*) Comparison of foveal red–green isoluminant and isochromatic contrast sensitivity for three human observers. The red–green isoluminant data have been slid upward by an amount corresponding to the difference in ideal contrast sensitivity for these two color directions. Solid arrows indicate the red–green isoluminant resolution limit and open arrows indicate the isochromatic resolution limit for each observer. (*Lower*) Ratio of human to ideal contrast sensitivity. Observers: NS, OP, and SG.

perceive the structure of these patterns. The ideal observer is agnostic about the appearance of spatial patterns and, therefore, provides an incomplete evaluation of the impact of optical stages on resolution. For example, the ideal observer analysis revealed that the packing geometry of receptors has little or no impact on ideal contrast sensitivity and that the only effect of varying receptor density is to produce a vertical shift in the ideal CSF. However, it is well known that packing geometry and density can strongly influence the aliasing artifacts that can plague imaging systems.

Fig. 8 shows an example of aliasing produced by an electronic still camera. The camera had a trichromatic sampling array not fundamentally different from the human retina; it contained a single charge-coupled device array in

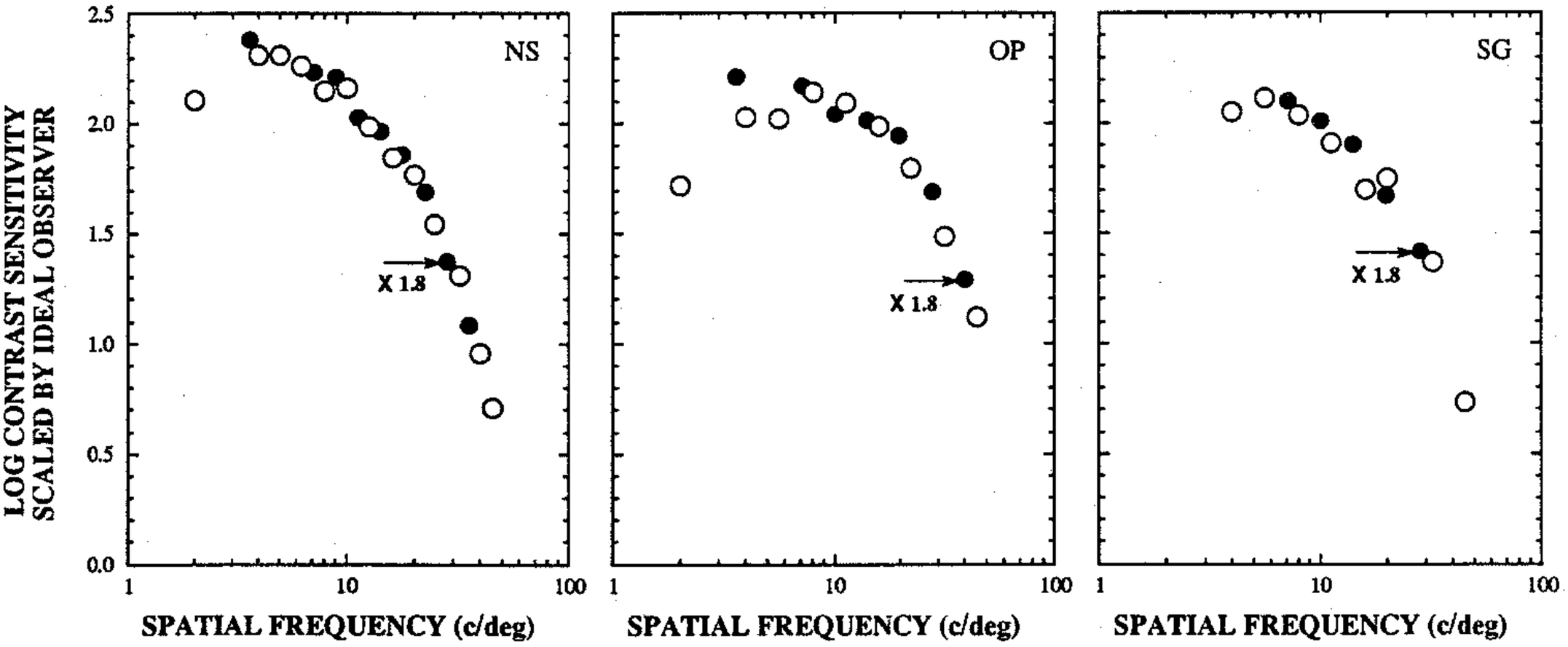

FIG. 5. Contrast sensitivity data of Fig. 6, but with the red–green isochromatic abscissa multiplied by a factor of 1.8 (slid rightward by 0.25 log unit). c/deg, Observers: NS, OP, and SG.

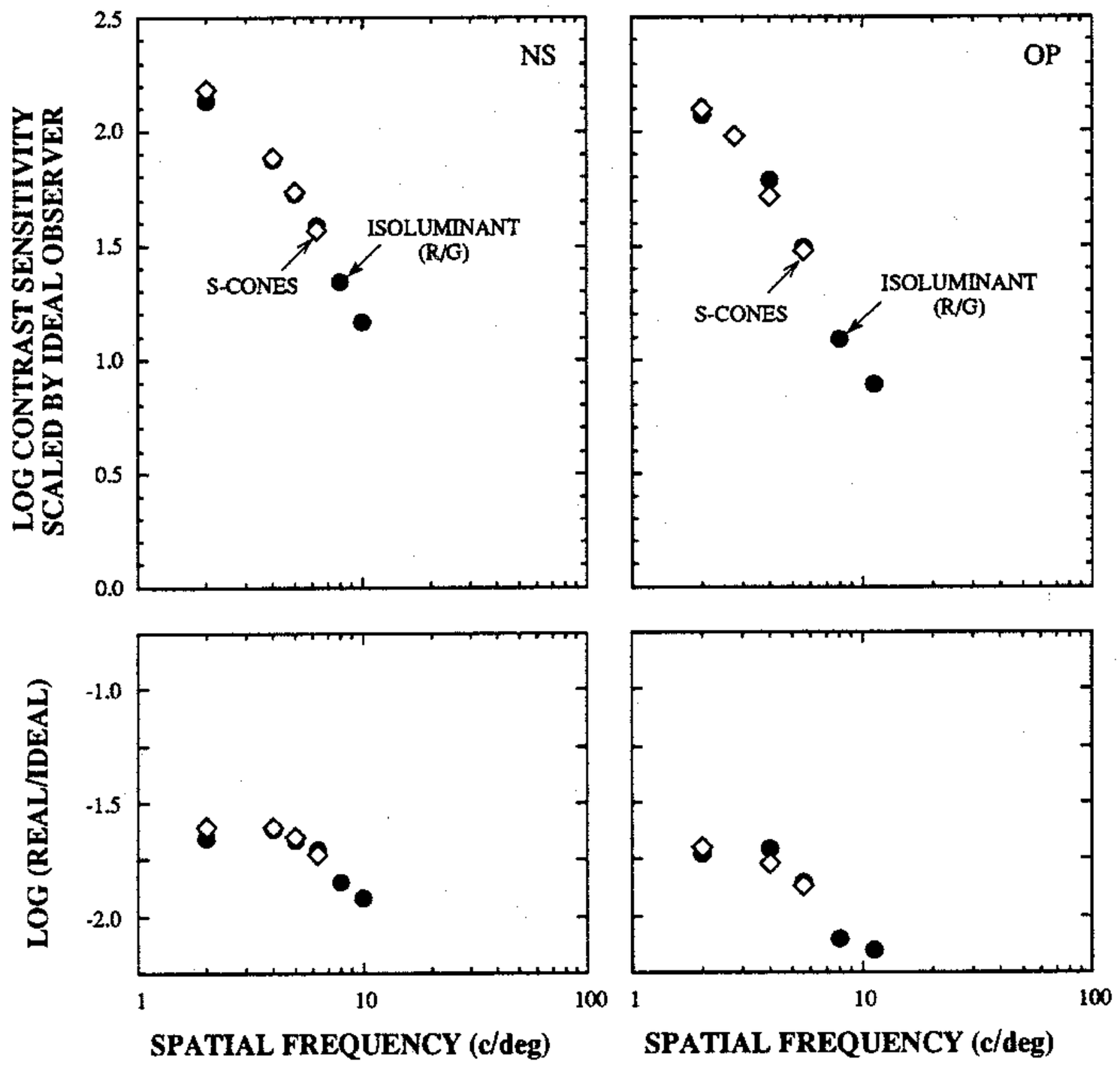

FIG. 6. (*Upper*) S-cone contrast sensitivity data for two observers in the parafoveal retina (1 degree eccentric) compared with red–green isoluminant contrast sensitivity at the same location. The S-cone data have been slid vertically upward by the difference in the contrast sensitivity of the ideal observer for these two color directions. (*Lower*) Ratio of human to ideal contrast sensitivity. Obsevers: NS and OP.

which each pixel was covered with one of three colored filters. The image is degraded by a chromatic moiré pattern as well as color distortion where there are highlights. These distortions arise because the spacing of each of the three sampling arrays in the charge-coupled device array is too large to faithfully represent the fine detail in the original scene.

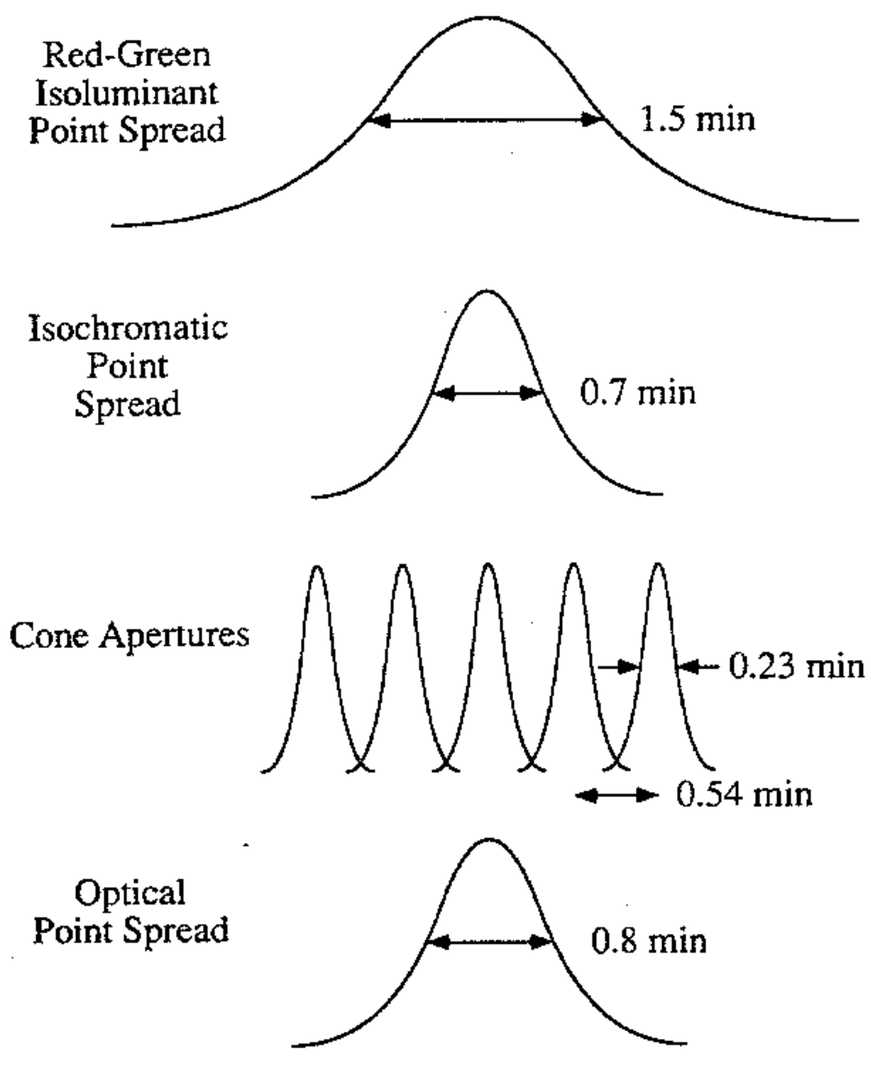

FIG. 7. Hypothetical neural point spread functions for the foveal detection of red–green isoluminant fringes and isochromatic fringes compared with estimates of the aperture and spacing of foveal cones and the point spread function of the optics of the eye.

There is considerable direct evidence for such sampling limitations in human vision [for a review, see Williams (19)]. Williams (20, 21) showed that observers viewing interference fringes with spatial frequencies exceeding the cone Nyquist frequency see coarse wavy patterns that resemble zebra stripes. He showed that these patterns are aliases of the original stimulus produced by the cone mosaic. Brewster (22) described a phenomenon in which fine black and white gratings appear to contain broad splotches of pastel hues. Williams *et al.* (23) established that this phenomenon is directly analogous to the chromatic distortions shown in Fig. 8. They found stimulus conditions in which Brewster's colors were produced by chromatic aliasing in the M- and L-cone mosaics. Sekiguchi *et al.* (3) found additional evidence for aliasing by these submosaics when observing red–green isoluminant interference fringes that exceeded the resolution limit. Williams and Collier (24) found stimulus conditions that produced chromatic aliasing by the S-cone mosaic alone.

One of the reasons aliasing usually cannot be seen in ordinary viewing conditions is that the optics of the eye attenuate these spatial frequency components in the retinal image before sampling by the cone mosaic. Fig. 9 *Upper* shows the modulation transfer function (MTF) of the eye's optics measured in collaboration with Rafael Navarro (Instituto de Optica, Madrid). These data are the mean MTFs for three observers, obtained with paralyzed accommodation and a 3-mm artificial pupil imaged in the plane of the natural pupil. A full account of the technique, which is a modified

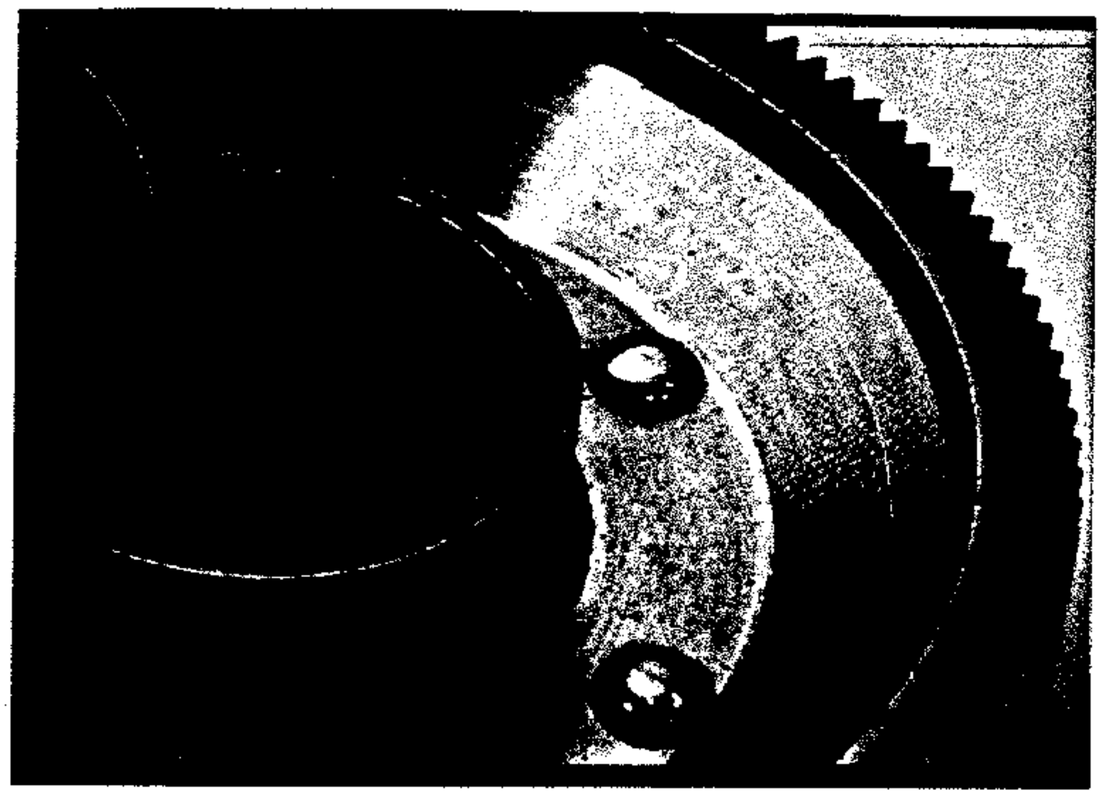

FIG. 8. Chromatic aliasing produced by an electronic still camera with a three-color charge-coupled device array.

version of that used by Campbell and Green (25), will be published elsewhere. Forced-choice contrast sensitivity measurements were made for interference fringe stimuli and incoherent gratings of the same wavelength (632.8 nm). The ratio of incoherent to coherent CSFs gave the MTF. The MTF has dropped by more than an order of magnitude at the Nyquist frequency for the combined M- and L-cone mosaics, shown by the dotted line (21). Outside the fovea, the retina is less well protected by the optics since optical quality remains high (26) despite a dramatic decline in the cone

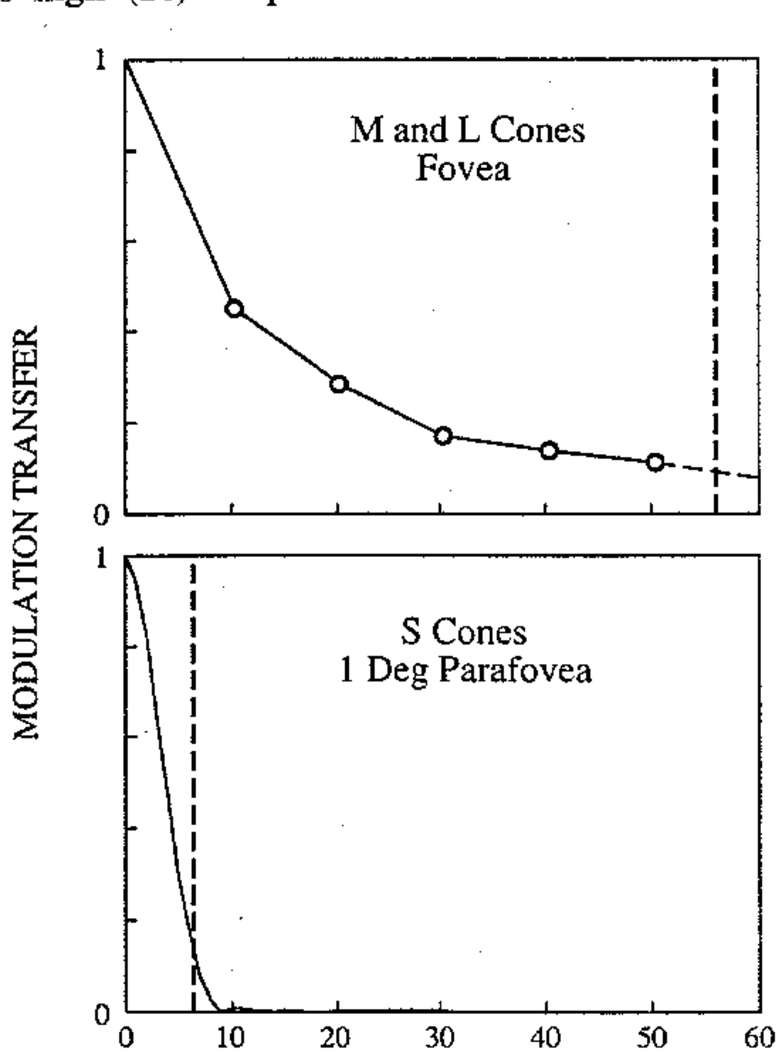

FIG. 9. (*Upper*) Foveal monochromatic MTF measured with laser interferometry compared with the foveal cone Nyquist frequency indicated by the dotted line. (*Lower*) Foveal MTF for the S cones, assuming diffraction and chromatic aberration are the only sources of image blur, compared with the S-cone Nyquist frequency indicated by the dotted line.

Nyquist frequency. Though aliasing can be seen there under normal viewing conditions, it is not usually seen, probably because the environment does not typically contain the high-contrast high-spatial-frequency stimuli that are required to see it (27).

Interestingly, the S cones seem to be protected from chromatic aliasing by the optics of the eye in much the same way as the cones as a whole (28). The eye suffers from chromatic aberration and it typically focuses in the long part of the visible spectrum, producing a high-contrast retinal image for the L and M cones. Under these circumstances, the retinal image is severely blurred in the short end of the spectrum to which S cones are sensitive. No direct measurements of the MTF of the retinal image seen by S cones have been made, but Fig. 9 *Lower* shows an estimate of the MTF, based on a model eye that suffers only from diffraction and the axial chromatic aberration. We assumed that the S cones were exposed to an equal energy spectrum and that the eye was focused at 555 nm. At the Nyquist frequency for the S-cone mosaic (10), indicated by the dotted line, chromatic aberration has severely attenuated the contrast of the retinal image available to the S cones, reducing the risk of aliasing. Patterns that are near the observer when the eyes are refracted for distant objects could partially correct for the deleterious effects of chromatic aberration. For example, a grating displayed in white light should produce maximum contrast for the S cones when the eye is accommodated to a distance that is ≈1 diopter beyond the grating. In this situation, S-cone aliasing can be seen in ordinary viewing (23).

The individual M- and L-cone submosaics are not so well protected, and it is not yet clear why chromatic aliasing by these cone classes is not a more prominent feature of everyday visual experience. One possibility is that eye movements help to reduce aliasing (29). When an object moves across the retina the chromatic alias changes with each retinal position. However, the correct interpretation of the image is invariant with retinal location. It may be that this invariance allows the visual system to overcome chromatic aliasing.

The CSFs calculated for the ideal observer are insensitive to aliasing effects because the ideal discriminator has exact knowledge of the stimulus. The ideal observer's performance depends only on whether the observed pattern of photon

catches is consistent with the stimulus or not. (Aliasing ambiguity would be relevant only if the fringe had an alias that was a uniform field. This would prevent the ideal observer from correctly deciding which interval contained the stimulus and which interval contained the uniform field, but it is a very unlikely situation.) The human observer, on the other hand, has neural mechanisms that dictate which interpretation will be perceived among the set of aliases generated by the cone mosaic. This tends to modify the human CSF when the cone Nyquist frequency is exceeded. Williams (20) showed that the foveal CSF for isochromatic interference fringes is modified by aliasing in the frequency range above the cone Nyquist frequency (≈60 cycles per degree). It is extended to frequencies as high as 150 cycles per degree because observers can detect moiré patterns (aliases) formed between the fringe and their own cone mosaic. Under optimal conditions, resolution for isochromatic interference fringes lies in the range of 50–60 cycles per degree, near the Nyquist frequency. Apparently the visual system lacks the neural machinery to provide veridical perception of an interference fringe when its frequency exceeds the Nyquist frequency.

Due to similar aliasing considerations, our conclusion that neural contrast sensitivity is the same for the two isoluminant color directions (red–green and S cone) does not imply that visual resolution is the same for S-cone stimuli as for red–green isoluminant stimuli. On the contrary, we find that they differ by roughly a factor of two. The arrows along the abscissa of Fig. 4 show that the resolution for red–green isoluminant gratings is between 20 and 27 cycles per degree, depending on the observer. Reports of the resolution of S-cone gratings are variable (24, 30–33) but are typically ≈10 cycles per degree and have never exceeded 16 cycles per degree (34). One reason for the difference in resolution is that only M and L cones and not S cones lie at the foveal center (35, 36) where the neural efficiency is presumably highest. A second reason may involve the lower sampling rate of the S cones compared with the M and L cones. When the S-cone Nyquist frequency is exceeded, observers begin to detect aliasing. Ultimately, the aliasing becomes more salient than the original signal and may interfere with resolution, i.e., choosing the correct interpretation of the stimulus. The M and L cones have substantially higher Nyquist frequencies, so aliasing does not intrude at such low frequencies, and resolution for red–green isoluminant gratings can exceed that for S-cone stimuli.

We thank Christine Curcio and Hugh Perry for supplying images of primate photoreceptor mosaics; Matt McMahon, Bill Haake, and Al Russell for technical assistance; and Rafael Navarro for help with the MTF measurements. This project was supported by Grants EY01319 and EY04367 from the National Institues of Health and AFOSR 88-6292 from the Air Force Office of Scientific Research.

1. Mullen, K. T. (1985) *J. Physiol.* **359,** 381–400.
2. Geisler, W. S. (1989) *Psychol. Rev.* **96,** 267–314.
3. Sekiguchi, N., Williams, D. R. & Brainard, D. H. (1993) *J. Opt. Soc. Am.* **10,** 2105–2117.
4. Sekiguchi, N., Williams, D. R. & Brainard, D. H. (1993) *J. Opt. Soc. Am.* **10,** 2118–2133.
5. Krauskopf, J., Williams, D. R. & Heeley, D. W. (1981) *Vision Res.* **22,** 1123–1131.
6. Williams, D. R. (1985) *J. Opt. Soc. Am. A:* **2,** 1087–1093.
7. Wyszecki, G. & Stiles, W. S. (1982) *Color Science* (Wiley, New York).
8. MacLeod, D. I. A., Williams, D. R. & Makous, W. (1992) *Vision Res.* **32,** 347–363.
9. Chen, B., Makous, W. & Williams, D. R. (1993) *Vision Res.* **33,** 413–427.
10. Curcio, C. A., Allen, K. A., Sloan, K. R., Lerea, C. L., Hurley, J. B., Klock, I. B. & Milam, A. H. (1991) *J. Comp. Neurol.* **312,** 610–624.
11. Baylor, D. A., Nunn, B. J. & Schnapf, J. L. (1987) *J. Physiol.* **390,** 145–160.
12. Snyder, A. W. & Miller, W. H. (1977) *J. Opt. Soc. Am.* **67,** 696–698.
13. Yellott, J. I. (1982) *Vision Res.* **22,** 1205–1210.
14. Yellott, J. I. (1983) *Science* **221,** 382–385.
15. Williams, D. R., Collier, R. J. & Thompson, B. J. (1983) in *Colour Vision Physiology and Psychophysics*, eds. Mollon, J. D. & Sharpe, L. T. (Academic, London), pp. 487–503.
16. Jordan, J. R., Geisler, W. S. & Bovik, A. C. (1990) *Vision Res.* **30,** 1955–1970.
17. Banks, M. S., Geisler, W. S. & Bennett, P. J. (1987) *Vision Res.* **27,** 1915–1924.
18. Westheimer, G. (1986) in *Handbook of Perception and Human Performance*, eds. Boff, K. R., Kaufman, L. & Thomas, J. O. (Wiley, New York), pp. 4.1–4.20.
19. Williams, D. R. (1992) in *Tutorials in Optics*, ed. Moore, D. T. (Optical Soc. Am., Washington, DC), pp. 15–28.
20. Williams, D. R. (1985) *Vision Res.* **22,** 195–203.
21. Williams, D. R. (1988) *Vision Res.* **28,** 433–454.
22. Brewster, D. (1832) *London Edinburgh Philos. Mag. J. Sci.* **1,** 169–174.
23. Williams, D. R., Sekiguchi, N., Haake, W., Brainard, D. & Packer, O. (1991) in *From Pigments to Perception*, eds. Valberg, A. & Lee, B. B. (Plenum, New York), pp. 11–22.
24. Williams, D. R. & Collier, R. (1983) *Science* **221,** 385–387.
25. Campbell, F. W. & Green, D. G. (1965) *J. Physiol.* **181,** 576–593.
26. Navarro, R., Artal, P. & Williams, D. R. (1993) *J. Opt. Soc. Am.* **10,** 201–212.
27. Galvin, S. J. & Williams, D. R. (1992) *Vision Res.* **32,** 2251–2259.
28. Yellott, J. I., Wandell, B. & Cornsweet, T. (1984) in *Handbook of Physiology: The Nervous System III*, ed. Darien-Smith, I. (Am. Physiol. Soc., New York), pp. 257–316.
29. Maloney, L. T. (1988) *Invest. Ophthalmol. Vis. Sci. Suppl.* **29,** 58 (abstr.).
30. Stiles, W. S. (1949) *Documenta Ophthalmol.* **3,** 138–163.
31. Green, D. G. (1968) *J. Physiol. (London)* **196,** 415–429.
32. Brindley, G. S. (1954) *J. Physiol. (London)* **124,** 400–408.
33. Cavonius, C. R. & Estevez, O. (1975) *J. Physiol.* **248,** 649–662.
34. Stromeyer, C. F., Kranda, K. & Sternheim, C. E. (1978) *Vision Res.* **18,** 427–437.
35. Williams, D. R., MacLeod, D. I. A. & Hayhoe, M. M. (1981) *Vision Res.* **21,** 1341–1356.
36. Williams, D. R., MacLeod, D. I. A. & Hayhoe, M. M. (1981) *Vision Res.* **21,** 1357–1375.